https://doi.org/10.48048/tis.2023.6793

Effect of Mg on Al-Mg Alloy and Electroless Ni-P Codeposition of nano-Al_2O_3: Mechanical, Wear, and Corrosion Resistance Properties

Shetha Daniel[1,*], Nilotpal Banerjee[1], Manik Majumder[1] and Sudhir Chitrapady Vishweshwara[2]

[1]Department of Mechanical Engineering, National Institute of Technology, Durgapur, India
[2]Department of Mechanical & Industrial Engineering, College of Engineering, National University of Science and Technology, Muscat, Oman

([*]Corresponding author's e-mail: shethamanu80@gmail.com)

Received: 27 February 2023, Revised: 3 April 2023, Accepted: 5 April 2023, Published: 28 July 2023

Abstract

The addition of magnesium to Aluminum alloys has become increasingly popular due to their lightweight, high strength, and corrosion resistance properties. Our research on high-content Mg doped 90, Al-10 wt% Mg alloy has shown that coating it with electroless Ni-P and codepositing nano-Al_2O_3 (0, 2.5, 5 and 7.5 wt%) can significantly improve its mechanical properties, resistance to wear & tear, and even corrosion resistance. The electroless Ni-P-5 wt% Al_2O_3 composite displayed a wear rate of 0.65×10^{-3} g/m at 12 N, a microhardness value of 598 HV, and remarkable thermal shock resistance. A strong and uniform bond was formed between the coating and substrate, and no delamination or cracking was observed. Polarisation curves in 3.5 wt% NaCl solution showed that the corrosion potential of the 90, Al-10 wt% Mg alloy was higher than that of Ni-P and Ni-P-nano Al_2O_3 composites, indicating that the incorporation of nano-Al_2O_3 into the Ni-P electroless bath provides superior corrosion protection. This cost-effective and simple approach makes the Ni-P-5 wt% Al_2O_3 nanocomposite coating an ideal choice for shielding Al-Mg alloys from corrosion.

Keywords: Al-Mg alloy, Electroless Ni-P composite coatings, Codeposition of nano Al_2O_3, Microstructure, Mechanical, Wear, Corrosion properties

Introduction

Aluminum alloys have a wide range of uses due to their interesting mechanical and physical properties [1,2]. Their composition is relatively simple, but they can be processed to achieve a number of microstructures and associated properties [3]. Generally, Al alloys are characterized by their high strength-to-weight ratio, good ductility, and excellent mechanical properties [2,4-6], making them an attractive option for a variety of applications, such as aerospace and automotive components [4,7]. However, limited anti-corrosion and wear resistance properties have made them less desirable in certain applications [8-12]. To improve the properties of Al alloys, researchers have added Mg to the alloy mixture, creating a stronger and more stable microstructure [13-15] while reducing impurities' solubility in the grain boundaries and improving mechanical properties [12]. Magnesium also has a lower melting point than aluminum, increasing overall strength and reducing corrosion [16]. Adding Mg to Al alloys is also cost-effective as it is less expensive than other metals [16]. Apart from alloy composition, there are different strategies to improve the performance of Al-Mg alloys, such as applying coatings and surface treatments such as thermal spraying, physical vapor deposition, chemical vapor deposition, plasma spray coatings, nitriding, and laser cladding [17-23]. These methods can help to reduce or prevent surface defects, improve wear resistance and reduce corrosion. One of the most cost-effective and effective coating processes for Al-Mg alloys is electroless nickel-phosphorus (Ni-P) coating [24-26]. This process provides a thin, uniform barrier against corrosion, reduces the coefficient of friction, and can be used to repair damaged surfaces. The composition of the deposit can be adjusted by varying the concentrations of the nickel salts and phosphoric in the solution, making it an ideal surface treatment for aluminum-magnesium alloys.

Furthermore, to enhance the performance of Ni-P coatings, nanoparticles are often added to the electroless plating solution [26-29]. These nanoparticles can improve the adhesion of the coating to the substrate, as well as its hardness and wear resistance. Furthermore, nanoparticles such as TiO_2, Al_2O_3, SiO_2, SiC, Si_3N_4, TiC, WO_3 etc., can also increase the corrosion resistance of Ni-P coatings [29-35]. Using nano-Al_2O_3 particles as an abrasion agent is an inexpensive and efficient way to improve a

material's hardness and chemical stability. The small size of the nano-Al_2O_3 particles makes them able to penetrate the substrate, and their high hardness allows them to remove material from the surface effectively. Further research is needed to study the electroless Ni-P-Al2O3 coating on Al-Mg alloy substrate [36-38]. Although a few reports have been conducted in this area, more work is required to gain a complete understanding of the process and its potential applications. Further studies are also needed to improve our knowledge of this plating process.

Moreover, further work is also needed to explore the potential applications of this technology [36-38]. This study used Ni-P electroless codeposition to deposit nano Al_2O_3 onto an Aluminium-Magnesium (90, Al-10 wt% Mg) alloy substrate. This study aimed to investigate the effect of Ni-P electroless codeposition of nano Al_2O_3 incorporated Al-Mg alloy on the mechanical and corrosion properties. The as-deposited coatings were characterized by X-ray diffraction (XRD), Scanning Electron Microscopy (SEM), Energy-Dispersive X-ray Spectroscopy (EDS), Vickers hardness test, and potentiodynamic polarization test.

Experimental method

In this work, a 90, Al-10 wt% Mg alloy substrate is prepared using the die-cast method. The alloy is composed of 90 wt% aluminum and 10 wt% magnesium. The mixture is heated until it reaches liquid and then poured into a mold to create the desired shape. The mold is then cooled, and the alloy solidifies. The resulting product is a substrate with a 90, Al-10 wt% Mg alloy composition. The alloy is composed of a high percentage of aluminum, which gives it good strength and corrosion resistance, and a small percentage of magnesium, which improves the mechanical properties of the alloy. Then it is cut into a $20\times10\times5$ mm^3 shape and polished with no-500 and 1,000 SiC paper. The alloy was rinsed with deionized water and immersed in an alkaline solution. The solution was then removed, and the alloy was placed in an oven at 65 degrees Celsius for 5 min. After 5 min, the alloy was removed from the oven and cooled to room temperature, and then the alloy was immersed in a chromic acid (CrO_3 20 g/100 mL) solution for acid pickling for 1 min. The final step was to immerse the alloy in a hydrofluoric acid solution (3.8 /100 mL) for activation treatment for about 10 min; in each step, the substrate was cleaned with deionized water. An electroless Ni-P bath was prepared by adding 35 g/L $NiSO_4.6H_2O$, 35 g/L lactic acid, 30 g/L $Na_2H_2PO_2.H_2O$, 10 g/L NH_4HF_2, 3 mg/L stabilizing agent, pH 6.5, and temperature 85 °C to a hot plate stirrer at 350 rpm. The approximately 50 nm nano-Al_2O_3 particles introduced to the bath were placed under an ultrasonic sonicator for 5 min before being transferred to a hot plate stirrer to create a homogenous mixture.

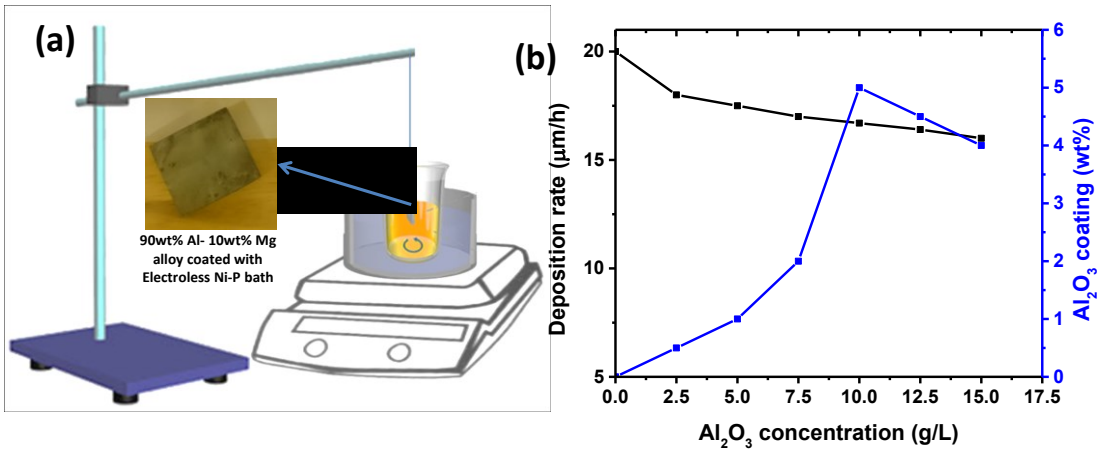

Figure 1 (a) Experimental setup (inset shows the specimen image of 90, Al-10 wt% Mg alloy coated with Electroless Ni-P bath and (b) experimental parameters of electroless Ni-P-Al_2O_3 coating on 90, Al-10 wt% Mg alloy.

Figure 1(a) shows the schematic illustration electroless deposition process. The tests for deposition rate and stability of plating baths are important for ensuring the quality of the final product. These tests help to optimize the conditions under which the plating process is performed and to ensure that the process is stable and reproducible. The deposition rate is determined by measuring the thickness of the

deposited film, and the stability of the plating bath is determined by measuring the concentrations of the metals in the bath. The deposition rate is expressed by the following equation:

$$D = \Delta w \times \frac{10^4}{pSt}$$

where D, Δw, p, S, t are deposition rate (μm/h), coating weight (g), the density of the Ni-P coating (~ 7.9 g/cm^3), the surface area of the Mg substrate (cm^2), deposition time (h), respectively. **Figure 1(b)** demonstrates the relationship between the concentration of nano Al_2O_3 and the deposition rate and Al_2O_3 coating weight. As the concentration of nano Al_2O_3 increases, the deposition rate and Al_2O_3 coating weight also increase. This data is important because it helps to optimize the production of Ni-P-Al_2O_3 coatings. At 10 g/L of nano Al_2O_3 shows the optimum deposition and coating. The results show that the addition of aluminum oxide nanoparticles can significantly improve the deposit properties. However, an increase in the concentration of Al_2O_3 particles above 10 g/L leads to a decrease in the coating. This is due to aggregation and weakening of the co-deposition behavior Ni-P with Al_2O_3. The particles aggregate and form larger clusters, leading to a decrease in the number of particles that can be deposited onto the substrate. In addition, particle aggregation decreases the particles' mobility, making it more difficult to deposit them onto the substrate. Moreover, as shown in **Figure 1(b)**, using 5 wt% nano Al_2O_3 (10 g/L) in Ni-P results in a better coating and deposition rate. This is due to the fact that the nanoparticles can better disperse in the liquid and thus provide a more uniform coating. In addition, the nanoparticles also increase the reactivity of the liquid, which leads to a faster deposition rate. The coatings were characterized by X-ray diffraction (Bruker D8 Discovery with Cu K_α radiation (λ = 1.5406 Å), Scanning electron microscopy (ZEISS EVO MA 10 at 40 mA, 40 KV). A potentiodynamic polarization test was performed on an electrochemical analyzer (CH Instruments, CHI608E) using a 3-electrode configuration in 3.5 wt NaCl at room temperature. The sweeping rate was 5 m/s, and the potential was swept from −0.2 to 0.6 V vs. SCE. The micro-hardnesses of the Al-Mg alloy with various composite coatings were measured with an HXD-1000 micro-hardness tester equipped with a Vicker indenter at a load of 100 g and a durable time of 15 s.

Results and discussion

In order to investigate how nano-Al_2O_3 particles influence the structure of a Ni-P coating, the XRD patterns of a 90, Al-10 wt% Mg alloy, a Ni-P coating, and a Ni-P-5 wt% Al_2O_3 composite coating are examined in **Figure 2**. As shown in **Figure 2**, the 90, Al-10 wt% Mg alloy is well matched with the cubically structured aluminum corresponding ICSD PDF Reference code No: 98-002-1647 and the hexagonally structured magnesium corresponding ICSD PDF Reference code No: 98-005-1506. The diffraction angle of crystal planes in an alloy composed of 90, Al-10 wt% Mg alloy mainly concentrates in the range of twenty to 80 degrees. The XRD patterns exhibit strong peaks at 2θ = 38.47 ° (111), 44.7 ° (002), 65.1 ° (022), and 78.24 ° (113) for the cubic structured Al, while the peaks for the hexagonal Mg structured 2θ = 36.61 ° (011) are smaller but still present. The difference between these 2 structures could be due to their different electronic states or interaction between atoms in the 2 structures.

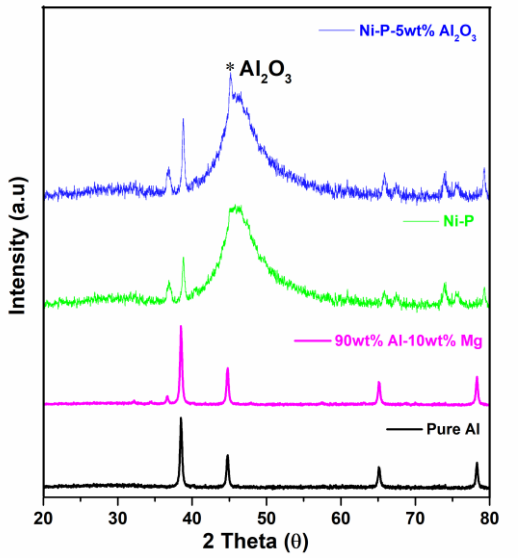

Figure 2 XRD profiles of 90, Al-10 wt% Mg alloy, electroless N-P, Ni-P-5 wt% Al_2O_3 coatings.

Further, the existence of a broad peak in the XRD profile indicates the formation of Ni-P coating with a mixed amorphous crystalline. The high-intensity diffraction that occurs at 44.7 ° can be attributed to the crystal plane (111) of a face-centered cubic (fcc) phase of nickel [39]. The peaks at around 2θ = 40 - 50 ° indicate the presence of Ni and P, respectively. The result also shows that there is fairly good coverage of Ni-P coatings on 90, Al-10 wt% Mg alloy. In addition to this, the XRD profile of a Ni-P-5 wt% nano-Al_2O_3 coating on top of a 90, Al-10 wt% Mg alloy reveals the presence of an amorphous phase in addition to the crystalline phases of nickel and aluminum. The presence of the Ni-P-5 wt% nano-Al_2O_3 coating is most likely to be responsible for the amorphous phase, whereas the crystalline phases are most likely attributable to the aluminum and magnesium substrate that lies beneath the coating. The diffraction peaks at 37.8 and 43.38 ° evidenced by Hexagonal structured Al_2O_3 corresponding to ICSD Reference code No: 98-003-2923. It was found that the diffraction peak of the (111) crystal plane shifts to 44.7 ° in Ni-P-5 wt% Al_2O_3 composite coatings when nano-Al_2O_3 particles are present on 90, Al-10 wt% Mg alloy. The shift of the (111) crystal plane might be due to the presence of nano-Al_2O_3 particles on the Ni substrate.

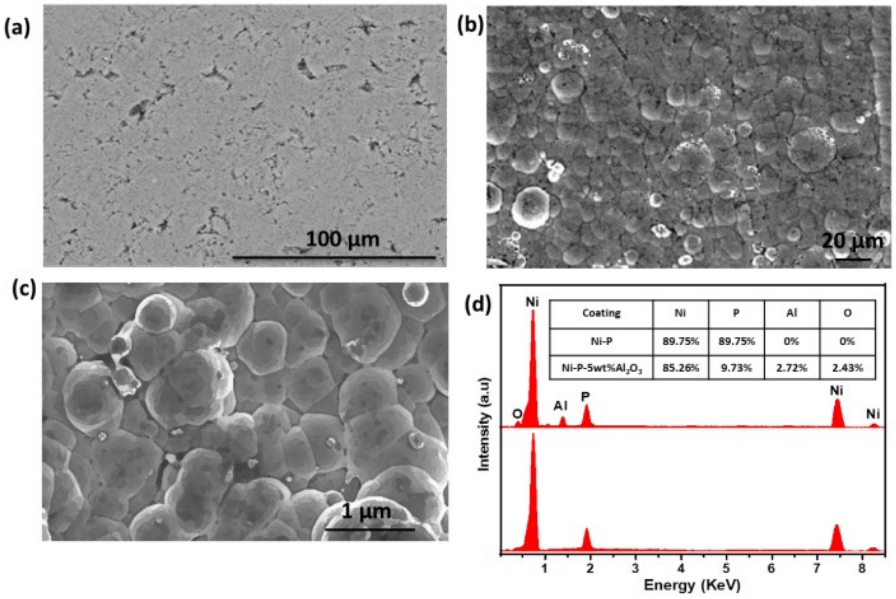

Figure 3 SEM images of (a) as cast 90, Al-10 wt% Mg, (b) N-P, (c) Ni-P-5 wt% Al_2O_3 electroless coatings on 90, Al-10 wt% Mg alloy, and (d) EDS spectra.

The change in surface morphology and SEM images of Al-Mg alloy were examined before and after the coating process in order to investigate the deposition process of Ni-P and Ni-P-5 wt% Al_2O_3 coatings on 90, Al-10 wt% Mg alloy. The SEM image of a 90, Al-10 wt% Mg alloy prepared by the die-cast method is shown in **Figure 3(a)**. The microstructure shows the irregular shape of particles and sharp edges. It was found that the as-cast surface was smooth and rough surface with many voids. The presence of voids in such composites is common due to the entrapping of air during the preparation process and the presence of the nano ceramic phase, which reduces the diffusion of metals [40]. This is due to the lack of nucleation sites for the Mg atoms to form their own phase. The Mg atoms are instead forced into the Al matrix, creating a brittle material [41]. After the Ni-P electroless coating, the surface became smoother with fewer voids and pores (**Figure 3(b)**). The Ni-P coating is uniform and well-adhered to the substrate, with no evidence of delamination, cracking, or gaps. The surface roughness of the coating is similar to that of the substrate, indicating good conformal coverage [42]. Ni-P coating typically presents a dense and nodular surface structure. This is due to the fact that Ni-P coatings are typically applied using electrodeposition, which results in the deposition of relatively large particles onto the surface. These particles then coalesce to form the characteristic nodular structure. The surface may also exhibit a rough or granular appearance in some cases. This is usually due to the presence of smaller particles that cannot coalesce into larger ones. When looking at the SEM images (**Figure 3(c)**) of Ni-P-5 wt% Al_2O_3 coated on Al-Mg alloy, one can see that the coating is very uniform and smooth. There are no visible pores or defects in the coating, which indicates that it is of high quality. The bright spots in the image are the result of the aluminum oxide that is being emitted from the surface of the alloy. The dark spots are due to nickel and phosphorus in the coating [37]. The average nodular size of Ni-P-5 wt% Al_2O_3 composite coatings is apparently higher than that of Ni-P coatings. This may be due to the presence of Al_2O_3 in the composite coatings, which acts as a barrier to the growth of the Ni-P crystals [43].

The smaller Al_2O_3 crystal size results in a more uniform and smoother surface finish. This effect is most likely due to the difference in solubility between Al_2O_3 and Ni-P in the coating. The smaller crystals have a larger surface area to volume ratio, increasing their reactivity with the surrounding environment and resulting in a more homogeneous coating. The EDS spectra of electroless Ni-P and Ni-P-5 wt% Al_2O_3 composites are shown in **Figure 3(d)**. The Ni-P spectrum is dominated by the peaks for Ni and P. The Ni-P-5 wt% Al_2O_3 spectrum is similar, but with the addition of a peak for Al and O. This indicates that the Al_2O_3 is present in the composite. The Ni-P-5 wt% Al_2O_3 composite shows a higher concentration of aluminum than the Ni-P composite, indicating that the aluminum has been evenly distributed throughout the composite.

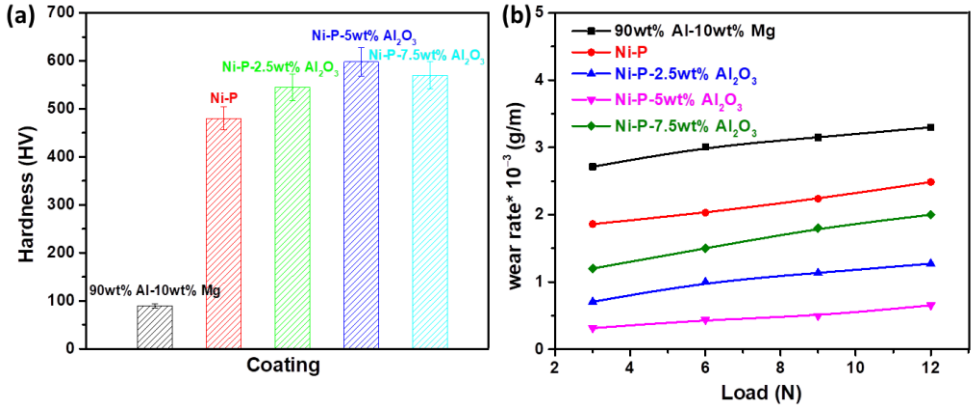

Figure 4 (a) Vickers hardness and (b) wear rate of the coatings.

Further, the coatings were subjected to a Vickers hardness test in order to determine their micro-hardness (**Figure 4(a)**). This test involved determining the average thickness of all the coatings, which was determined to be 18 µm and estimated based on the deposition rate and the deposition time. **Figure 4(a)** displays the findings of micro-hardness tests conducted on an alloy substrate consisting of 90, Al-10 wt% Mg alloy and coatings containing varying amounts of aluminum oxide. The micro-hardness of the bare 90, Al-10 wt% Mg alloy is only about 90 HV, as shown in **Figure 4(a)**. On the other hand, the micro-hardness of a 90, Al-10 wt% Mg alloy substrate coated with a Ni-P coating can reach up to 480 HV. Since it is approximately 390 HV higher than the substrate, this demonstrates that the Ni-P coating has the potential to improve the hardness of the substrate coating effectively. In addition, the

microhardness of coatings made of Ni-P-Al_2O_3 composites tends to increase significantly as the percentage of Al_2O_3 present in the coating rises from 0 to 5 wt% as the coating is applied. As a result, Ni-P-5 wt% nano-Al_2O_3 composite coatings display the highest hardness value, measured at 598 HV. This is due to the synergistic combination of Ni, P, and Al_2O_3 components, which optimizes the Ni-P alloy's phase structure and improves the mechanical properties of the coating (**Figure 3**) [44]. On the other hand, the micro-hardness of the coatings drops down to 570 HV even though the content of Al_2O_3 in the composite coatings increases to 7.5 wt% due to the increased porosity in the coating. This indicates that higher nanoparticle content can potentially affect the Ni-P crystal structures, which can result in the unfavourable performance of the composite coatings. The microhardness parameters obtained through experimentation are presented in **Table 1**.

Table 1 Experimental parameters of 90, Al-10 wt% Mg alloy substrate, the Ni-P coating, and the Ni-P-nano-Al_2O composite coatings.

Composites	Micro-hardness (HV)	i_{corr} (A/cm^2)	E_{corr} (V)
90, Al-10 wt% Mg	90	1.5×10^{-4}	−1.36
90, Al-10 wt% Mg with Ni-P coating	480	1.8×10^{-6}	−0.44
90, Al-10 wt% Mg with Ni-P-2.5 wt% nano-Al_2O_3 coating	545	7.2×10^{-7}	−0.39
90, Al-10 wt% Mg with Ni-P-5 wt% nano-Al_2O_3 coating	598	1.2×10^{-7}	−0.28
90, Al-10 wt% Mg with Ni-P-7.5 wt% nano-Al_2O_3 coating	570	5.2×10^{-7}	−0.33

The wear rate of 90, Al-10 wt% Mg, electroless Ni-P, Ni-P-2.5, Ni-P-5, and Ni-P-7.5 wt% Al_2O_3 nanocomposite coatings were measured under varying loads, as shown in **Figure 4(b)**. According to Archard's law, the wear rate increased linearly with increasing load, indicating abrasive wear. The penetration of wear debris and fracture of the top layer also accompanied the rise in wear rate [45]. The load applied resulted in more contact between the particles and the substrate and increased the normal force on the particles. With higher loads, the indentation of the material is analogous to the wear behavior, with an increase in the wear rate proportionally linked to the pin penetration depth and material removed. The Ni-P-5 wt% Al_2O_3 electroless composite demonstrated the lowest wear rate of all the composites. At a load of 12 Newtons, the Ni-P-5 wt% Al_2O_3 electroless coating had a wear rate of 0.65×10^{-3} g/m, compared to 3.31×10^{-3}, 2.48×10^{-3}, 1.27×10^{-3} and 2.1×10^{-3} g^4/m^4 for the Al-Mg, Ni-P, Ni-P-2.5 and Ni-P-7.5 wt% Al_2O_3 respectively. The superior wear resistance of the electroless Ni-P nano-5 wt% Al_2O_3 nanocomposite coating is attributed to its finer-grained structure [45,46], along with the added strength and hardness, which increases the resistance to sliding and reduces the plastic deformation of subsequent layers, thus reducing the amount of material removed and the wear rate [35,47,48].

Table 2 Comparison of microhardness and wear rate of 90, Al-10 wt% Mg alloy substrate coated with other composites.

Composites	Micro-hardness (HV)	Specific wear rate (g/m)	Ref
90, Al-10 wt% Mg with Ni-P-5 wt% nano-Al_2O_3	598	0.65×10^{-3}	This work
Al-10 % Mg - 5 % nano Al_2O_3	87	1.61×10^{-3}	[49]
Q235 steel with Ni-P-Al_2O_3	569	1.768×10^{-3}	[50]
Ni-P/SiC on AZ31	795	4.2×10^{-5}	[26]
Ni-P-W on AZ91	647	3.1×10^{-3}	[51]

Table 2 provides a comparison of the microhardness and wear rate of a 90, Al-10 wt% Mg alloy substrate when coated with Ni-P-5 wt% nano-Al_2O_3, which exhibits favourable performance. The increased surface energy associated with the presence of such composites likely contributes to improved tribological properties. In addition, the Mg particles and intermetallic phases between Al and Mg and the formation of a super saturated solid solution create a denser material and fill in the gaps between grains. The Al-Mg matrix formed over the grain boundaries strengthens the bonding between Ni-P-Al_2O_3 particles and the Al-Mg grain interface, resulting in better penetration impedance of the composite surface. Furthermore, the hardness and compressive strength are increased while maintaining the ductility

of the composite. This combination of properties may lead to extended life and improved performance for various components.

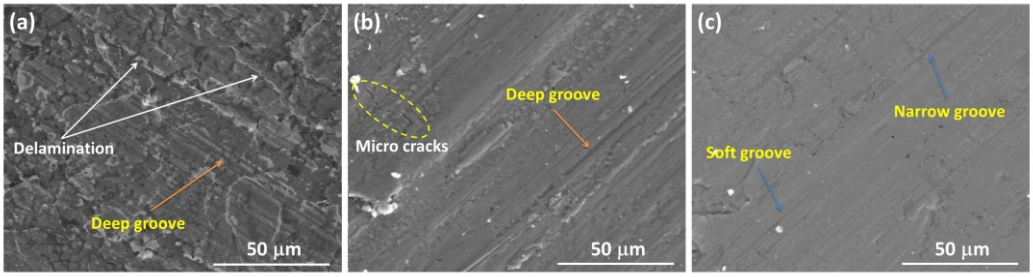

Figure 5 SEM of worn surface of (a) 90, Al-10 wt% Mg alloy, (b) Ni-P, and (c) the Ni-P-5 wt% Al_2O_3 composite coatings.

Worn surfaces were evaluated using SEM to determine the impact of electroless Ni-P addition and Al_2O_3 nano-particles on the wear response of a 90, Al-10 wt% Mg alloy (**Figure 5**). Groove width and depth are greater for the 90, Al-10 wt%Mg nanocomposites than the electroless coated Ni-P and NiP-5 wt% Al_2O_3 nanocomposites, even though the test load is the same for all 3. For the 90, Al-10 wt% Mg sample, delaminations are the major wear mechanism because of the separation of coarse debris into layers. This results in the formation of bigger grooves. The reduced hardness of 90, Al-10 wt% Mg compared to other samples allows deep penetration of the indenter during the wear test, separating coarse debris. Thin deformed sheets are created when coarse debris creating scratches and galling on the sample surface is removed in a direction parallel to the sliding direction. The larger debris here serves as an additional source of material removal, and wear rates are higher. In addition, the contact surface undergoes deformation, generating a thin layer with increased strains and temperatures as a result of wear pressures caused by siding as sliding contact time rises. Sliding further accumulates strains at these thin layers, causing their separation and the wear delamination mechanism. The wear-worn surface of a Ni-P nanocomposite is distinct from that of a 90, Al-10 wt% Mg composite, exhibiting smooth grooves and micro-cracks with less intense delaminations. Electroless Ni-P's coating hardness limits the indenter's penetration depth on the surface, leading to fine debris during sliding. Also, its motion is slowed when an indenter slides across a surface containing Ni or P nanoparticles. The absence of delamination in the microstructure is reflected in the Ni-P-5 wt% Al_2O_3's weathered surface. In composites, only microscopic cracks can be seen. Strength and scratch resistance are also enhanced by the smaller crystallite size of these composites compared to 90, Al-10 wt% Mg and Ni-P nanocomposites. Additionally, the bonding between Al_2O_3 particles and the Al-Mg grain interface is enhanced by creating a Ni-P-5 wt% Al_2O_3 electroless coating across the grain boundaries, leading to improved penetrating resistance of the composite surface. Because of these 2 factors, the sub-layers beneath the indenter do not undergo deformation, and delaminations do not form during the wear test; instead, microcracks at the surfaces of the samples become the primary wear mechanism, resulting in less material removal and better wear properties.

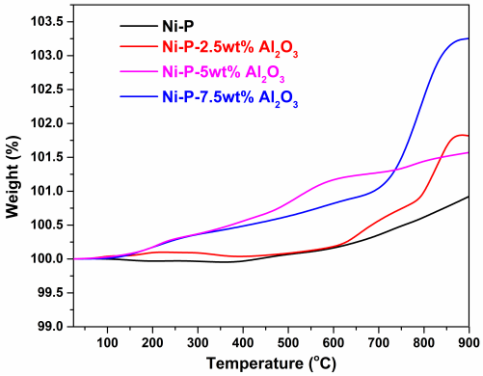

Figure 6 Thermogravimetric analysis of the 90, Al-10 wt% Mg alloy coated with electroless Ni-P and the Ni-P-nano-Al_2O composite coatings.

Thermogravimetric analysis (TGA) is a powerful analytical technique used to determine the weight loss of a material as a function of temperature or time. This technique can be used to investigate any chemical reaction or physical change that causes a change in the mass of the material. The developed composite coatings were analyzed using the TGA method, and the results were presented in **Figure 6**, showing the weight loss as a function of temperature. The data obtained from the TGA analysis showed that the mass of the composites increased with temperature, which indicates the formation of a reaction between the materials comprising the Al-Mg alloy and Ni-P-Al_2O_3 coating eutectic [28]. This suggests that, upon heating, Ni-P-Al_2O_3 and the Al, Mg atoms rearrange themselves to form a new, more thermodynamically stable compound. The weight loss in all coated samples is below 1 %, which suggests that the coating is thermally stable and uniformly distributed. This is an important property for a coating, as it will not degrade under normal use conditions.

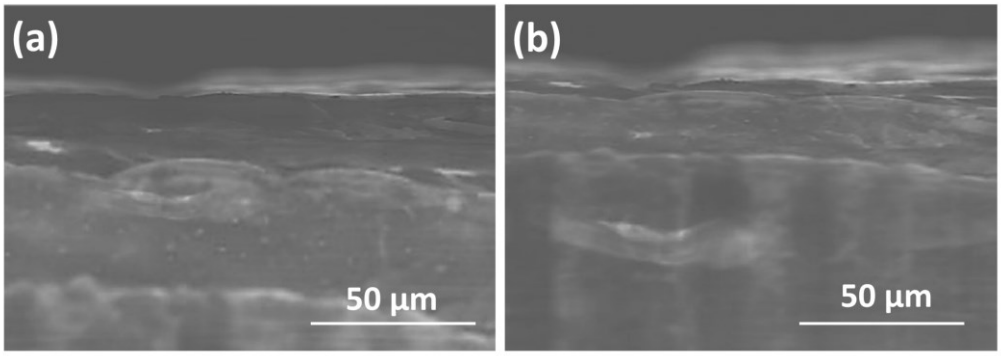

Figure 7 Cross-section SEM images of the (a) Ni-P coating and (b) Ni-P-5 wt% nano-Al_2O_3 composite coatings on 90, Al-10 wt% Mg alloy substrate during a thermal shock test.

Further, a thermal shock test was performed to evaluate the adhesion of coatings. This test determines how well a material can withstand sudden temperature changes. The test results will help determine whether or not the coating is suitable for use in applications where it will be exposed to extreme temperatures. The substrate composed of 90, Al-10 wt% Mg, along with Ni-P and Ni-P-nano-Al_2O_3 composites, is loaded into a high-temperature furnace and heated to 250 °C. After that, it was put under ice water to stop the reaction, and this process was repeated 20 times. The results showed that the coatings had good adhesion and no sign of delamination or cracking. The SEM cross-section images of the thermal shock samples show no apparent defects between the coatings (**Figure 7**). The cross-section observations indicate that nano-Al_2O_3 is well distributed in the matrix, and no delamination is observed. The lack of defects suggests that the coatings could withstand thermal shock without damage. This is an important finding, showing that the coatings effectively protect the underlying material from thermal stress.

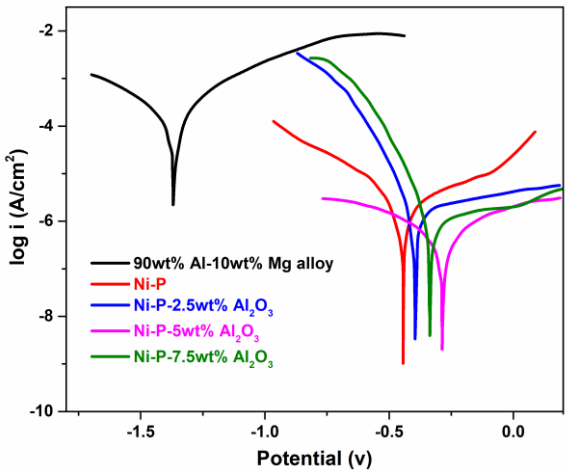

Figure 8 Polarization curves of the 90, Al-10 wt% Mg alloy coated with electroless Ni-P and the Ni-P-nano-Al_2O composite coatings.

Figure 8 and **Table 1** show the corrosion potential and current density of 90, Al-10 wt% Mg alloy, Ni-P coating, and Ni-P-nano-Al_2O_3 composite coatings in a 3.5 % NaCl solution. The cathode reaction in the polarization curves corresponds to the hydrogen evolution, while the anodic polarization curves are the most important characteristic of corrosion resistance. The anodic polarization curves of metals can be used to predict their corrosion behavior in various environments. The shape of the anodic polarization curve is determined by the metal-oxygen reaction's kinetics and the oxygen solubility in the metal. The polarization curves reveal that the corrosion potential of 90, Al-10 wt% Mg alloy is more negative than that of Ni-P and Ni-P-nanoAl_2O_3 composites, indicating that codeposition of nano-Al_2O_3 of Ni-P electroless coating in Al-Mg alloys are more resistant to corrosion in this solution. **Figure 6** shows pure 90, Al-10 wt% Mg alloy shows the lowest corrosion potential (E_{corr} = −1.36 V) and highest corrosion current density (i_{corr} = 1.5×10^{-4} A/cm^2). In addition, the Ni-P coating that was applied to the 90, Al-10 wt% Mg alloy substrate caused E_{corr} to shift more toward the positive side, reaching −0.044 V, and i_{cor} reach 1.8×10^{-6} A/cm^2. In addition, when we raised the concentration of nano-Al_2O_3 in the Ni-P bath from 2.5 to 5 wt%, the alloy showed the highest E_{corr} = −0.28V and the lowest i_{corr} = 1.2×10^{-7} A/cm^2, respectively (**Table 1**). This is due to the homogeneous distribution of nano-Al_2O_3 in Ni-P and the uniform coating on the surface of the substrate without any pores and cracks (**Figure 3**).

Furthermore, the concentration of nano-Al_2O_3 rose from 5 to 7.5 wt%, and the values of i_{corr} and E_{corr} changed to −0.33 V and 5.2×10^{-7} A/cm^2 as a result of the increase in porosity of the coating. These findings show the Al_2O_3 content of composite coatings has an important effect on corrosion resistance. The Al_2O_3 forms a barrier layer on the surface of the coating, which protects the underlying substrate from corrosion. The 5 wt% Al_2O_3 content, the thicker and more protective the barrier layer will be on the Al-Mg substrate.

Conclusions

This study aimed to analyze the impact of electroless Ni-P and codeposition of nano-Al_2O_3 (0, 2.5, 5, and 7.5 wt%) on a high magnesium content alloy composed of 90, Al-10 wt% Mg. The effects on the Al-Mg alloy's microstructure, mechanical, wear, and corrosion properties were analyzed. The incorporation of nano-Al_2O_3 particles in the Al-Mg alloy matrix resulted in improved mechanical and corrosion resistance. Scanning electron microscope (SEM) revealed a distributed coating in the Al-Mg matrix. The micro-hardness test showed that the hardness of the 90, Al-10 wt% Mg alloy enhanced with rising nano- Al_2O_3 content. Adding 5 wt% nano-Al_2O_3 to the Ni-P bath in the 90, Al-10 wt% Mg alloy resulted in a 664 % hardness enhancement and 0.65×10^{-3} g/m wear rate at 12 N. This combination of wear and hardness resistance is believed to be a consequence of Al_2O_3 particles in the Ni-P matrix, providing a hard phase and hindrance to avoid wear debris from cutting into the softer Ni-P matrix. Additionally, the thermal shock test confirmed good thermal stability for the 90, Al-10 wt% Mg alloy coated by including nano-Al_2O_3 particles in the Ni-P bath. The polarization curves indicated that by introducing nano-Al_2O_3 in the Al-Mg alloy, it had an increased resistance to corrosion in a 3.5 wt% NaCl solution.

References

[1] T Dursun and C Soutis. Recent developments in advanced aircraft aluminium alloys. *Mater. Des.* 2014; **56**, 862-71.

[2] E Georgantzia, M Gkantou and GS Kamaris. Aluminium alloys as structural material: A review of research. *Eng. Struct.* 2021; **227**, 111372.

[3] M Grimm, A Lohmüller, RF Singer and S Virtanen. Influence of the microstructure on the corrosion behaviour of cast Mg-Al alloys. *Corrosion Sci.* 2019; **155**, 195-208.

[4] D Varshney and K Kumar. Application and use of different aluminium alloys with respect to workability, strength and welding parameter optimization. *Ain Shams Eng. J.* 2021; **12**, 1143-52.

[5] RP Verma and MK Lila. A short review on aluminium alloys and welding in structural applications. *Mater. Today Proc.* 2021; **46**, 10687-91.

[6] MN Su and B Young. Material properties of normal and high strength aluminium alloys at elevated temperatures. *Thin Walled Struct.* 2019; **137**, 463-71.

[7] A Heinz, A Haszler, C Keidel, S Moldenhauer, R Benedictus and WS Miller. Recent development in aluminium alloys for aerospace applications. *Mater. Sci. Eng. A* **2000**; 280, 102-7.

[8] R Qiu, Z Li and Z Wu. Enhanced anti-icing and anticorrosion properties of wear-resistant superhydrophobic surfaces based on Al alloys. *Mater. Res. Express* 2019; **6**, 045059.

[9] Y Liu, M Liu, X Chen, Y Cao, HJ Roven, M Murashkin, RZ Valiev and H Zhou. Effect of Mg on microstructure and mechanical properties of Al-Mg alloys produced by high pressure torsion. *Scripta Mater.* 2019; **159**, 137-41.
[10] L Zhang, Z Cao, Y Liu, G Su and L Cheng. Effect of Al content on the microstructures and mechanical properties of Mg-Al alloys. *Mater. Sci. Eng. A.* 2009; **508**, 129-33.
[11] D Drozdenko, J Čapek, B Clausen, A Vinogradov and K Máthis. Influence of the solute concentration on the anelasticity in Mg-Al alloys: A multiple-approach study. *J. Alloy. Comp.* 2019; **786**, 779-90.
[12] S Gaurav, R Mishra and M Zunaid. A critical review on mechanical and microstructural properties of dissimilar aluminum (Al)-magnesium (Mg) alloys. *J. Adhes. Sci. Tech.* 2022; **37**, 1117-49.
[13] M Peron, J Torgersen and F Berto. Mg and its alloys for biomedical applications: exploring corrosion and its interplay with mechanical failure. *Metals* 2017; **7**, 252.
[14] F Barandehfard, J Aluha, A Hekmat-Ardakan and F Gitzhofer. Improving corrosion resistance of aluminosilicate refractories towards molten Al-Mg alloy using non-wetting additives: A short review. *Materials* 2020; **13**, 4078.
[15] XM Zhang and WP Chen. Review on corrosion-wear resistance performance of materials in molten aluminum and its alloys. *Trans. Nonferrous Met. Soc. China* 2015; **25**, 1715-31.
[16] DS Kumar, CT Sasanka, K Ravindra and K Suman. Magnesium and its alloys in automotive applications-a review. *Am. J. Mater. Sci. Tech.* 2015; **4**, 12-30.
[17] J Zhang, B Song, Q Wei, D Bourell and Y Shi. A review of selective laser melting of aluminum alloys: Processing, microstructure, property and developing trends. *J. Mater. Sci. Tech.* 2019; **35**, 270-84.
[18] M Daroonparvar, HR Bakhsheshi-Rad, A Saberi, M Razzaghi, AK Kasar, S Ramakrishna, PL Menezes, M Misra, AF Ismail and S Sharif. Surface modification of magnesium alloys using thermal and solid-state cold spray processes: Challenges and latest progresses. *J. Magnes. Alloy.* 2022; **10**, 2025-61.
[19] R Kromer, S Costil, C Verdy, S Gojon and H Liao. Laser surface texturing to enhance adhesion bond strength of spray coatings-Cold spraying, wire-arc spraying, and atmospheric plasma spraying. *Surf. Coating. Tech.* 2018; **352**, 642-53.
[20] LA Dobrzański. *Effect of heat and surface treatment on the structure and properties of the Mg-Al-Zn-Mn casting alloys*. Magnesium and Its Alloys. 1st ed. CRC Press, Florida, 2019.
[21] AA Siddiqui and AK Dubey. Recent trends in laser cladding and surface alloying. *Optic. Laser Tech.* 2021; **134**, 106619.
[22] ZZ Yin, WC Qi, RC Zeng, XB Chen, CD Gu, SK Guan and YF Zheng. Advances in coatings on biodegradable magnesium alloys. *J. Magnes. Alloy.* 2020; **8**, 42-56.
[23] A Jung, A Buchwalder, E Hegelmann, P Hengst and R Zenker. Surface engineering of spray-formed aluminium-silicon alloys by plasma nitriding and subsequent electron beam remelting. *Surf. Coating. Tech.* 2018; **335**, 166-72.
[24] M Yan, H Ying and T Ma. Improved microhardness and wear resistance of the as-deposited electroless Ni-P coating. *Surf. Coating. Tech.* 2008; **202**, 5909-13.
[25] J Balaraju, TS Narayanan and S Seshadri. Electroless Ni-P composite coatingsJ. Appl. Electrochem. 2003; **33**, 807.
[26] N Ghavidel, SR Allahkaram, R Naderi, M Barzegar and H Bakhshandeh. Corrosion and wear behavior of an electroless Ni-P/nano-SiC coating on AZ31 Mg alloy obtained through environmentally-friendly conversion coating. *Surf. Coating. Tech.* 2020; **382**, 125156.
[27] I Thakur, V Pandey, P Rao, S Tyagi and D Goyal. Tribological study of mechanically milled graphite nanoparticles codeposited in electroless Ni-P coatings. *Met. Powder Rep.* 2020; **75**, 344-9.
[28] P Chandrasekar and D Nagaraju. The effects of electroless Ni−P-Coated SiC and Al_2O_3 on wear behaviour and thermal stability of AMMCs. *Arabian J. Sci. Eng.* 2022; **47**, 15603-12.
[29] VB Chintada and R Koona. Influence of SiC nano particles on microhardness and corrosion resistance of electroless Ni-P coatings. *J. Bio Tribo Corrosion* 2018; **4**, 68.
[30] M Gholizadeh-Gheshlaghi, D Seifzadeh, P Shoghi and A Habibi-Yangjeh. Electroless Ni-P/nano-WO_3 coating and its mechanical and corrosion protection properties. *J. Alloy. Comp.* 2018; **769**, 149-60.
[31] DR Dhakal, G Gyawali, YK Kshetri, JH Choi and SW Lee. Influence of SiC and TiC nanoparticles reinforcement on the microstructure, tribological, and scratch resistance behavior of electroless Ni-P coatings. *Nanotechnology* 2019; **31**, 104001.

[32] DR Dhakal, YK Kshetri, B Chaudhary, TH Kim, SW Lee, BS Kim, Y Song, HS Kim and HH Kim. Particle-size-dependent anticorrosion performance of the Si_3N_4-nanoparticle-incorporated electroless Ni-P coating. *Coatings* 2021; **12**, 9.
[33] DF Carrillo, A Bermudez, MA Gomez, AA Zuleta, JG Castano and S Mischler. Fretting-corrosion behavior of electroless Ni-P/Ni-P-TiO_2 coatings obtained on AZ91D magnesium alloy by a chromium-free process. *Surface. Interfac.* 2020; **21**, 100733.
[34] M Islam, MR Azhar, N Fredj, TD Burleigh, OR Oloyede, AA Almajid and SI Shah. Influence of SiO_2 nanoparticles on hardness and corrosion resistance of electroless Ni-P coatings. *Surf. Coating. Tech.* 2015; **261**, 141-8.
[35] A Sharma and A Singh. Electroless Ni-P and Ni-P-Al_2O_3 nanocomposite coatings and their corrosion and wear resistance. *J. Mater. Eng. Perform.* 2013; **22**, 176-83.
[36] P Chandrasekar and D Nagaraju. The effect of electroless Ni–P-Coated Al_2O_3 on mechanical and tribological properties of scrap Al alloy MMCs. *Int. J. Metalcasting* 2022; **17**, 356-72.
[37] A Arumugam, P Lakshmanan, S Palani and K Parthiban. Wear behavior of Ni-P and Al_2O_3 electroless nano coating on aluminium alloy. *Mater. Today Proc.* 2021; **46**, 1066-70.
[38] M Lakavat, A Bhaumik, S Gandi and SR Parne. Electroless Ni-P-B coatings on magnesium alloy AZ91D: Influence of nano Al_2O_3 on corrosion, wear, and hardness behaviour. *Surf. Topogr. Metrology Properties* 2022; **10**, 025021.
[39] S Guo, L Hou, C Guo and Y Wei. Characteristics and corrosion behavior of nickel-phosphorus coatings deposited by a simplified bath. *Mater. Corrosion* 2017; **68**, 468-75.
[40] V Ingle and M Sorte. Defects, root causes in casting process and their remedies. *Int. J. Eng. Res. Appl.* 2017; **7**, 47-54.
[41] X Li, W Xia, H Yan, J Chen, B Su, M Song, Z Li and Y Li. Dynamic recrystallization behaviors of high Mg alloyed Al-Mg alloy during high strain rate rolling deformation. *Mater. Sci. Eng. A* 2019; **753**, 59-69.
[42] SHM Anijdan, M Sabzi, MR Zadeh and M Farzam. The effect of electroless bath parameters and heat treatment on the properties of Ni-P and Ni-P-Cu composite coatings. *Mater. Res.* 2018; **21**, e20170973.
[43] EM Fayyad, AM Abdullah, MK Hassan, AM Mohamed, G Jarjoura and Z Farhat. Recent advances in electroless-plated Ni-P and its composites for erosion and corrosion applications: A review. *Emergent Mater.* 2018; **1**, 3-24.
[44] S Karthikeyan and B Ramamoorthy. Effect of reducing agent and nano Al_2O_3 particles on the properties of electroless Ni-P coating. *Appl. Surf. Sci.* 2014; **307**, 654-60.
[45] JP Davim. *Tribology for engineers: A practical guide*, Elsevier, 2011.
[46] S Alirezaei, S Monirvaghefi, M Salehi and A Saatchi. Wear behavior of Ni-P and Ni-P-Al_2O_3 electroless coatings. *Wear* 2007; **262**, 978-85.
[47] JP Davim. *Progress in green tribology: Green and conventional techniques*. De Gruyter, Germany, 2017.
[48] JP Davim. *Wear of advanced materials*. John Wiley & Sons, New York, 2013.
[49] M Eltaher, A Wagih, A Melaibari, A Fathy and G Lubineau. Effect of Al_2O_3 particles on mechanical and tribological properties of Al-Mg dual-matrix nanocomposites. *Ceram. Int.* 2020; **46**, 5779-87.
[50] Y Li, K Zhang, M Zhang, Y Zhang, T Wu, H Zhao, J Su, Z Wang and J Wang. Preparation of sol-enhanced Ni–P–Al_2O_3 nanocomposite coating by electrodeposition. *J. Nanomaterials* 2020; **2020**, 5239474.
[51] S Taşci, RC Özden and M Anik. Corrosion and wear characteristics of electroless Ni–P, Ni–P–W and composite Ni–P–W/Al_2O_3 coatings on AZ91 Sheet. *Met. Mater. Int.* 2019; **25**, 313-23.